JOURNAL OF MODERN OPTICS, 20 JANUARY–15 FEBRUARY 2005
VOL. 52, NO. 2–3, 185–199

Taylor & Francis
Taylor & Francis Group

Molecular tunnelling ionization and rescattering induced double ionization of H_2 and D_2 molecules

X. M. TONG†, Z. X. ZHAO† and C. D. LIN†‡

†J. R. Macdonald Laboratory, Physics Department,
Kansas State University, Manhattan, KS 66506, USA
‡Physics Division, National Center for Theoretical Sciences,
PO Box 2-131, Hsinchu, 30013, Taiwan

(*Received 17 March 2004; revision received 3 April 2004*)

Abstract. We review the recently developed molecular tunnelling ionization theory, which is an extension of the well-known tunnelling model for atoms, by taking into account the characteristic of molecular orbitals. Employing the molecular tunnelling theory and the rescattering model, we have studied the double ionization of D_2 and H_2 molecules by intense lasers. Comparing our calculated kinetic energy release spectra of D^+ with the measured data, we can derive the time duration between the first and second ionizations to sub-femtosecond accuracy and the breakup distance of D_2 to within a fraction of one Angstrom.

1. Introduction

When a D_2 molecule is exposed to an intense laser pulse, the D^+ ion spectra from the kinetic energy release (KER) offers a way to study the dynamics of the D_2 breakup. (Note that the analysis is also valid for H_2. We take D_2 as an example in order to compare with experiment.) The measured KER spectra of D^+ contains the time duration ('molecular clock') between the first and second ionization and the nuclear separation when the D_2 breaks up. By comparing the KER spectra from circularly and linearly polarized laser fields, the high energy part of the KER spectra has been attributed to ionization of D_2^+ by the rescattering mechanism [1–4]. To confirm that the rescattering model indeed works and to be able to extract the time and distance information from the measured KER spectra, we need to theoretically evaluate all the dynamical processes leading to the breakup of the D_2 molecule when it is exposed to a laser pulse.

In figure 1 we depict the physical processes according to the rescattering mechanism that lead to the breakup of the D_2 molecule. Following figure 1, a D_2 molecule is ionized near the peak field of the laser pulse at t_0. This ionization launches two correlated wave packets: an electronic wave packet which is driven by the combined laser field and the Coulomb field of the D_2^+ ion, and a vibrational nuclear wave packet which is assumed to propagate freely in the σ_g ground potential of D_2^+. The vibrational wave packet at t_0 is taken to be the ground vibrational state of D_2, assuming the Frank–Condon principle. For $t > t_0$, the

Journal of Modern Optics ISSN 0950–0340 print/ISSN 1362–3044 online © 2005 Taylor & Francis Ltd
http://www.tandf.co.uk/journals
DOI: 10.1080/09500340410001725568

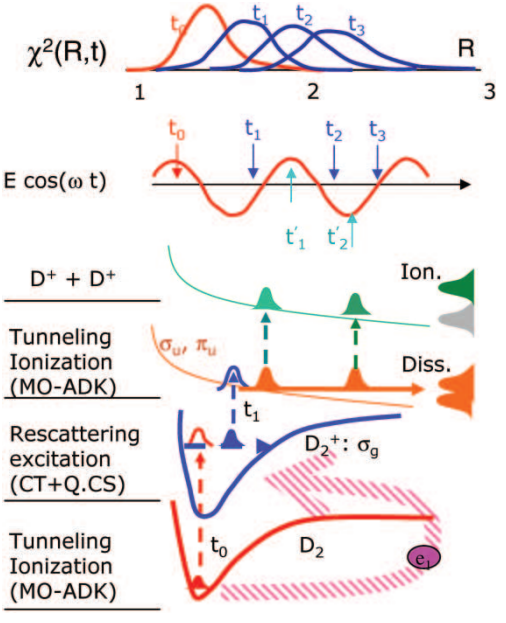

Figure 1. Schematics of the major physical processes leading to the formation of the D^+ ion. The D_2 is first ionized at t_0 creating an electron wave packet which returns to collide with D_2^+ at time t_1. In the meanwhile, the initial vibrational wave packet, created at t_0 and measured by $\chi^2(R, t)$, would move to larger R and broaden at later time. At t_1, the D_2^+ is excited from σ_g to σ_u and π_u molecular states by electron impact. The excited D_2^+ can dissociate directly to give $D^+ + D$, or further ionized at t'_1, t'_2, etc., to produce two D^+ ions by Coulomb explosion. Note that similar rescattering processes can be initiated at later time, t_2, t_3, etc., and are included in the simulated D^+ spectra.

vibrational wave packet propagates outward and broadens, as shown in the top frame of figure 1. The electron initially is driven out by the laser field but returns after 2/3 of an optical cycle to recollide with D_2^+ at time t_1. The rescattering can excite D_2^+ to higher electronic states or to ionize it. Once the D_2^+ is in the excited electronic state, it can dissociate or it can be further ionized by the laser field. Since the laser pulse lasts for many optical cycles, the electron can revisit the D_2^+ ion many cycles later after the initial ionization. Thus rescattering can occur on the second return at t_2, on the third return at t_3, etc., see figure 1. For each initial t_0, the return times t_1, t_2, t_3, ... are fairly well defined. Since the initial ionization at t_0 occurs only in a sub-fs time interval, the rescattering times t_i ($i = 1, 2, 3, \ldots$) are also defined at the sub-fs (or atto-second) accuracy. If the rescattering populates only the lowest excited electronic state, σ_u and then the D_2^+ dissociates, the peaks of the D^+ kinetic energy release can be used to read the clock at the rescattering times, as depicted in figure 1.

To read out the dynamical information from the measured KER spectra, we need to understand (1) the tunnelling ionization process and (2) the rescattering process. We will review the molecular tunnelling ionization theory and the rescattering model in section 2. The results from the simulation and comparison with the experiment are given in section 3, followed by a short summary.

2. Theoretic method

2.1. *Molecular tunnelling ionization theory*

The Ammosov–Delone–Krainov (ADK) [5–7] tunnelling ionization theory has been shown to provide a simple and efficient way to estimate the ionization rate of an atom in a strong laser field. The key ingredients in the theory are the ionization potential and the angular momentum of the valence electron. In the molecular case, the angular momentum is not a good quantum number. One has to take into account the molecular symmetry when deriving the molecular tunnelling theory (MO-ADK). The ADK theory for ionization of atoms in a laser field is based on the tunnelling of an electron through the suppressed potential barrier of the combined atomic field and the external electric field. For a static electric field and a hydrogenic atom the tunnelling rate can be calculated analytically. The ADK theory is obtained by modifying the analytical formula by including the effect from the non-hydrogenic radial wavefunction of the valence electron in the asymptotic region where tunnelling occurs. To obtain tunnelling ionization rates for molecules, similar considerations on the electronic wave functions in the asymptotic region have to be considered. Since the ADK model for atoms was derived for an electronic state with a well-defined spherical harmonics, to obtain ionization rates for molecules, one has to express the molecular electronic wave functions in the asymptotic region in terms of summations of spherical harmonics in a one-centre expansion.

In the molecular frame, the asymptotic wave function of a valence electron in a diatomic molecule at large distances can be expressed as (atomic units $m = \hbar = e = 1$ are used throughout the paper unless otherwise indicated)

$$\Psi^m(\mathbf{r}) = \sum_l C_l F_l(r) Y_{lm}(\hat{\mathbf{r}}), \tag{1}$$

with m being the magnetic quantum number along the molecular axis. We normalize the coefficient C_l in such a way that the wave function in the asymptotic region can be expressed as

$$F_l(r \to \infty) \approx r^{Z_c/\kappa - 1} \exp(-\kappa r), \tag{2}$$

where Z_c is the effective charge, $\kappa = (2I_p)^{1/2}$ and I_p is the ionization potential for the given valence orbital. Here, we assume that the molecular axis is aligned along the external field direction. The valence electron will be ionized along the field direction at $\theta \sim 0$. The leading term of the spherical harmonic along this direction is

$$Y_{lm}(\hat{\mathbf{r}}) \simeq Q(l, m) \frac{1}{2^{|m|}|m|!} \sin^{|m|}\theta \frac{\exp(\mathrm{i}m\phi)}{(2\pi)^{1/2}}, \tag{3}$$

with

$$Q(l, m) = (-1)^m \left(\frac{(2l+1)(l+|m|)!}{2(l-|m|)!} \right)^{1/2}. \tag{4}$$

The wave function in the tunnelling region can be written as

$$\begin{aligned}\Psi^m(\mathbf{r}) &\simeq \sum_l C_l Y_{lm}(\hat{\mathbf{r}})\ r^{Z_c/\kappa-1}\ \exp(-\kappa r)\\ &\simeq \sum_l C_l Q(l,m) r^{Z_c/\kappa-1}\ \exp(-\kappa r)\frac{\sin^{|m|}\theta}{2^{|m|}|m|!}\frac{\exp(\mathrm{i}m\phi)}{(2\pi)^{1/2}}\\ &\simeq B(m) r^{Z_c/\kappa-1}\exp(-\kappa r)\ \frac{\sin^{|m|}\theta}{2^{|m|}|m|!}\frac{\exp(\mathrm{i}m\phi)}{(2\pi)^{1/2}},\end{aligned} \tag{5}$$

with

$$B(m) = \sum_l C_l Q(l,m). \tag{6}$$

Following the same procedure used in [5], we obtain the tunnelling ionization rate in a static field as

$$w_{\mathrm{stat}}(F,0) = \frac{B^2(m)}{2^{|m|}|m|!}\frac{1}{\kappa^{2Z_c/\kappa-1}}\left(\frac{2\kappa^3}{F}\right)^{2Z_c/\kappa-|m|-1}\exp(-2\kappa^3/3F). \tag{7}$$

Note that in equation (7) we have corrected the error in the coefficients in [5]. If there is only one partial wave l, equation (7) returns to the atomic case as shown in [6].

If the molecular axis is not aligned along the field direction, but at an arbitrary angle $\mathbf{R}$ with respect to the field direction, the $B(m)$ in equation (7) is expressed as

$$B(m') = \sum_l C_l D^l_{m',m}(\mathbf{R}) Q(l,m'), \tag{8}$$

with $D^l_{m',m}(\mathbf{R})$ being the rotation matrix and $\mathbf{R}$ being the Euler angles between the molecular axis and the field direction. The static field ionization rate is

$$w_{\mathrm{stat}}(F,\mathbf{R}) = \sum_{m'}\frac{B^2(m')}{2^{|m'|}|m'|!}\frac{1}{\kappa^{2Z_c/\kappa-1}}\left(\frac{2\kappa^3}{F}\right)^{2Z_c/\kappa-|m'|-1}\exp(-2\kappa^3/3F). \tag{9}$$

The ionization rate in a low frequency linearly polarized field is given by

$$w(F,\mathbf{R}) = \left(\frac{3F}{\pi\kappa^3}\right)^{1/2} w_{\mathrm{stat}}(F,\mathbf{R}). \tag{13}$$

where F is the peak field strength.

In the MO-ADK theory for each molecular orbital, one has to calculate the coefficients C_l and then the ionization rates can be obtained analytically for molecules. These coefficients have been obtained by the multiple-scattering method [8, 9] and their values at equilibrium distances have been tabulated for a few diatomic molecules [10]. One can obtain these parameters by fitting the valence electron wavefunction calculated by other methods as well. With the coefficients C_l obtained, one can study the tunnelling ionization rates for aligned [11, 12] as well as randomly oriented molecules [10]. Note that the present MO-ADK theory can in principle be easily extended to more complex compact polyatomic molecules, like SO_2 and NO_2, where the valence electron can still be approximated by the one-centre expansion. For large molecules, the MO-ADK model may not work well because of the slow convergence of the one-centre

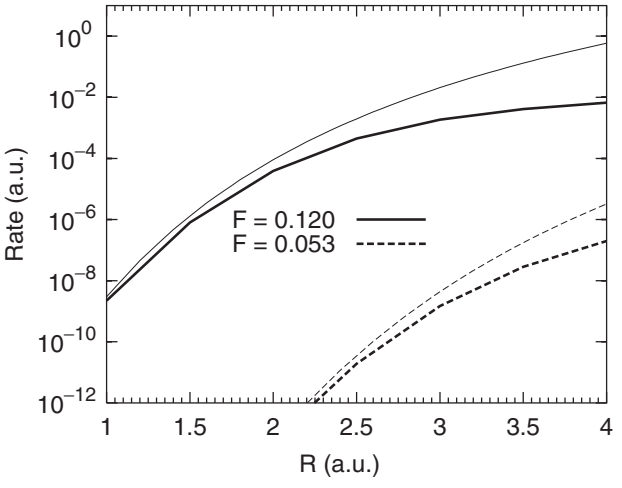

Figure 2. MO-ADK rates of D_2^+ in a static electric field. Thick lines are the 'exact' static ionization rates.

expansion. However, the MO-ADK theory has not been fully tested for polyatomic molecules so far.

2.2. *Validity of the MO-ADK theory*

Since the ADK model is based on a perturbative approach and the MO-ADK theory has a further one-centre expansion approximation on the molecular orbitals, we need to know its region of validity. For D_2^+ aligned parallel to the field direction, we show in figure 2 the static MO-ADK rate as compared to the 'exact' static tunnelling ionization rates calculated using the complex rotation method [13] at two field strengths. For small internuclear separations, the MO-ADK rates are quite close to the 'exact' ones. The MO-ADK rates tend to overestimate at large internuclear separations where the one-centre expansion of the molecular orbitals do not work as well. For most of the small diatomic molecules, the equilibrium distance is about 2.0 a.u. and MO-ADK should be valid for ionization from the ground states.

2.3. *The rescattering model*

Following the initial ionization of D_2, a correlated electron wave packet and a vibrational wave packet are created at t_0. The initial vibrational wave packet is taken to be the ground vibrational wavefunction of D_2, assuming that the ionization process is fast and the Frank–Condon principle is valid. Due to the heavy mass of the nuclei, the vibrational motion is not modified by the subsequent laser field. The time evolution of the vibrational wave packet is thus described by

$$\chi(R,t) = \sum_v C_v \chi_{\mathrm{v}}(R)\, \exp\left(-\mathrm{i}\varepsilon_v t\right), \tag{11}$$

$$C_v = \int \chi_{\mathrm{g}}(R)\chi_v(R)\, \mathrm{d}R. \tag{12}$$

Here $\{\chi_v(R)\}$ and $\{\varepsilon_v\}$ are the vibrational wavefunction and vibrational energy of D_2^+ in the σ_g ground electronic state, respectively, and $\chi_g(R)$ is the ground vibrational wavefunction of D_2.

The rescattering model for describing the motion of the ionized electron in the subsequent laser field is modelled similar to the method used by Yudin and Ivanov [14, 15] for He. The ionized electron is treated classically, under the combined force from the laser field and the residual Coulomb interaction from the D_2^+ ion. For simplicity, the latter is approximated by an effective charge $Z_c = +1$ at the midpoint of the internuclear axis. To calculate the trajectory of the ionized electron, we solve the equation of motion (Newton's second law), with the initial condition that the ionized electron is at $(x, y, z) = (0, 0, z_0)$ where z_0 is the tunnelling position from the combined potential of the Coulomb field and the static electric field. The initial velocity $\mathbf{v}$ is assumed to have a distribution from the ADK model,

$$g(\mathbf{v}) \propto \exp(-\mathbf{v}^2\kappa/F). \tag{13}$$

In this model, the tunnelled electron is ejected isotropically with a Gaussian distribution in velocity, i.e. we consider the ejected electron to have initial velocity in both the transverse and the longitudinal directions. For each initial time t_0 or phase ϕ_0 that the ionized electron was born, the classical equation of motion was solved to obtain the trajectory. The distance of the electron from the centre of the D_2^+ ion is monitored for over seven optical cycles for longer pulses or until the end of the laser pulse if the pulse is shorter. The distance of closest approach of the electron from the ion and the time when this occurs for each trajectory are recorded. From these data, the impact parameter b and the collision energy T of the corresponding electron–ion impact (no laser field) excitation or ionization are obtained.

Figure 3 shows the probability distribution of finding the returning electron with kinetic energy T measured in the asymptotic region for a laser with peak

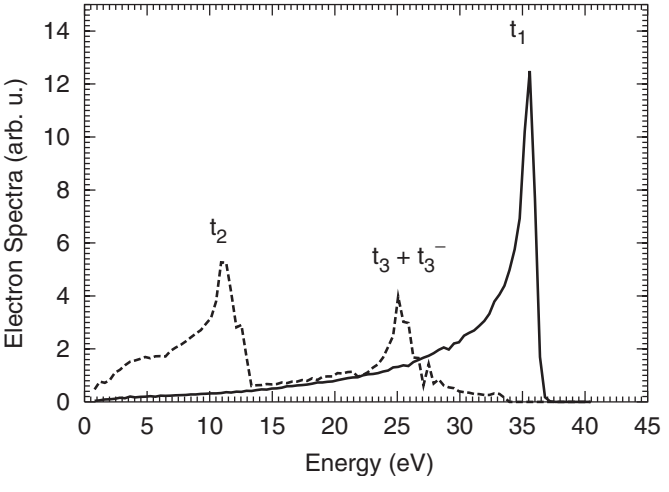

Figure 3. Returning electron energy spectra for D_2 in a pulse laser with peak intensity of $1.5\,I_0$ ($I_0 = 10^{14}\,\mathrm{W\,cm^{-2}}$) and pulse length of 40 fs obtained from the simulation.

intensity at $1.5\,I_0$. If the residual Coulomb interaction from the D_2^+ ion is neglected, the expected maximum returning energy will be $3.17\ U_P = 29\,\text{eV}$, where U_P is the Pondermotive energy. The inclusion of Coulomb interaction increases this peak energy to about 35 eV.

In figure 3 we show three groups of returning electrons. In the first group, the electron was born at t_0 when the laser field has a positive phase ϕ_0 (i.e. beyond the peak field). It was driven outward and then back by the oscillating laser field to recollide with the D_2^+ ion within one optical cycle. This group is denoted by t_1 where the returning electron has a peak current near 35 eV. The second group labelled t_2 denotes an electron which does not collide with the ion at the first return, but at the second return about half a cycle later after the electron reverses its direction again. The kinetic energy for this group of electrons is smaller. The third group was denoted by $t_3 + t_3^-$. For the t_3, the recollision occurs at the third return. For the t_3^- group, the electrons were born at a negative phase ϕ_0 [16], i.e. before the laser reaches the peak field. These negative phase electrons do not recollide with the ion in the first optical cycle when the field changes direction since they were accelerated by an increasing field right after birth. Due to the Coulomb focusing by the ion they collide with the ion at the third return. Without the Coulomb focusing the negative phase birth would not contribute to the rescattering process. In calculating the returning electron energy distribution shown in figure 3 proper weights from the MO-ADK rates and the initial velocity distribution of the tunnelling electron have been accounted for. In figure 3 we did not show the electron energy distributions from collisions which occurred at returns after two optical cycles. The general trend is that at higher returns, the kinetic energy of the electron is smaller and the probability of rescattering is also smaller. In our calculations we have accounted for rescattering up to seven optical cycles for the long laser pulses.

2.4. *Electron impact excitation and ionization probabilities*

For each impact parameter b and kinetic energy T of the returning electron, we need to calculate the electron impact excitation and ionization cross-sections of D_2^+ at each internuclear separation R. Different from the He^+ case, there are few experimental or theoretical data available for D_2^+. Thus we have to generate the cross-sections needed semi-empirically. For each total cross-section $\sigma(T)$ at kinetic energy T, we assume that the probability for excitation or ionization at impact parameter b is given by

$$P_m(b, T) = \sigma(T)\frac{\exp(-b^2/a_o^2)}{\pi a_o^2}, \tag{14}$$

$$a_o = (2/\Delta E)^{1/2}, \tag{15}$$

where $T = v^2/2$ and ΔE is the excitation or ionization energy. Here, the b dependence is taken to have the Gaussian form. For the rescattering in He, Yudin and Ivanov [14] have checked different forms of b dependence and concluded that the results are rather insensitive to the precise functional form used.

For electron impact ionization cross-section, we employ the empirical formula

$$\sigma_i(T, \Delta E) = \frac{\pi}{\Delta E^2} \exp\left(1.5(\Delta E - 0.5)/T\right) f(T/\Delta E), \tag{16}$$

$$f(x) = \left(A \ln x + B\left(1 - \frac{1}{x}\right) - C\frac{\ln x}{x}\right)\frac{1}{x}. \tag{17}$$

where ΔE is the ionization energy. The three terms in equation (17) represent electron impact ionization cross-section in the high-energy limit, low energy limit and for the intermediate energy region. By fitting this formula to the accurate theoretical H(1s) ionization cross-section [17] we obtained $A = 0.7213$, $B = -0.302$ and $C = 0.225$. The empirical formula, equation (16), is used to make sure that (i) the ionization cross-section is in good agreement with that of He^+ [17] for small internuclear separation; (ii) the ionization cross-section is in good agreement with that of H [17] for large internuclear separation; and (iii) the ionization cross-section of D_2^+ at equilibrium distance is in reasonable agreement with the recommended one from NIST [18]. Therefore equation (16) should be valid for any internuclear separations.

For the excitation process, it is clear that σ_u and π_u states will be the dominant channels populated via electron impact excitation from the ground σ_g state since they have the lowest excitation energies. There are no theoretical or experimental data available for such cross-sections as functions of internuclear separations. Thus we will employ a semi-empirical fitting procedure as well. We assume that the excitation cross-section again can be fitted in the form of equations (16) and (17) as in ionization, except that ΔE now is the excitation energy and the number 0.5 in equation (16) should be replaced by the excitation energy of the corresponding state in atomic hydrogen. From the tabulated $H(1s) \rightarrow H(2p)$ excitation cross-section by Bray [17], we obtained $A = 0.7638$, $B = -1.1759$ and $C = -0.6706$. The formula was further tested by comparing the predicted excitation cross-section with the calculated one for $e^- + He^+(1s) \rightarrow e^- + He^+(2p)$. From the total $1s \rightarrow 2p$ excitation cross-section, we can further distinguish the excitation cross-section to $2p_0$ or $2p_1$, with the direction of the incident electron beam as the quantization axis. The relative $2p_0$ and $2p_1$ cross-sections can be calculated theoretically or experimentally from polarization or correlation measurements. (Note: the $2p_{-1}$ cross-section is identical to the $2p_1$ cross-section by symmetry.) We fit the $2p_0$ to $2p_1$ cross-section ratio by

$$r(x) = \frac{\sigma_0}{\sigma_1} = \frac{8.2(1 + 1.1/x^2)^{1/2}}{x} + 0.44. \tag{18}$$

where $x = T/\Delta E$ is the scaled kinetic energy. Since the ratio for He does not differ much from the calculated ratio for H, this comparison convinces us to use the $r(x)$ in equation (18) to describe the ratio for D_2^+ as well. The $r(x)$ indicates that $m = 0$ is the dominant magnetic component in the present interested energy regime.

To relate the $2p_0$ or $2p_1$ partial cross-sections to the excitation cross-sections of σ_u and π_u electronic states of D_2^+, we need to know the alignment angle of the molecule. If the molecule is aligned along the laser field polarization direction (which is also the direction of the electron beam), the $2p_0$ cross-section is the excitation to the σ_u state and the $2p_1$ ($2p_{-1}$) cross-section is for the excitation to the π_u state. If the molecule is aligned perpendicular to the laser polarization direction, then the role is reversed, i.e. $2p_1$ (or $2p_{-1}$) corresponds to the cross-section of the

σ_u excitation, and the $2p_0$ cross-section to the π_u excitation. For any arbitrary alignment angle θ of D_2^+, we assume that the total excitation cross-sections to σ_u and π_u are given by

$$\sigma(\sigma_u) = \sigma_T(r_0 \cos^2 \theta + r_1 \sin^2 \theta), \tag{19}$$

$$\sigma(\pi_u) = \sigma_T(r_0 \sin^2 \theta + r_1 \cos^2 \theta), \tag{20}$$

$$\sigma_T = \sigma_0 + 2\sigma_1, \tag{21}$$

$$r_0 = \frac{\sigma_0}{\sigma_T} = \frac{r(x)}{r(x)+2}, \tag{22}$$

$$r_1 = \frac{2\sigma_1}{\sigma_T} = \frac{2}{r(x)+2}. \tag{23}$$

The semi-empirically fitted electron impact ionization or excitation cross-section formulae discussed so far are for a free electron colliding with an atomic or molecular ion. For the rescattering process, the two electrons in D_2 initially are in the singlet state ($S = 0$). Thus in principle, one should just use singlet excitation or ionization cross-sections, instead of the spin-averaged cross-sections. We obtain

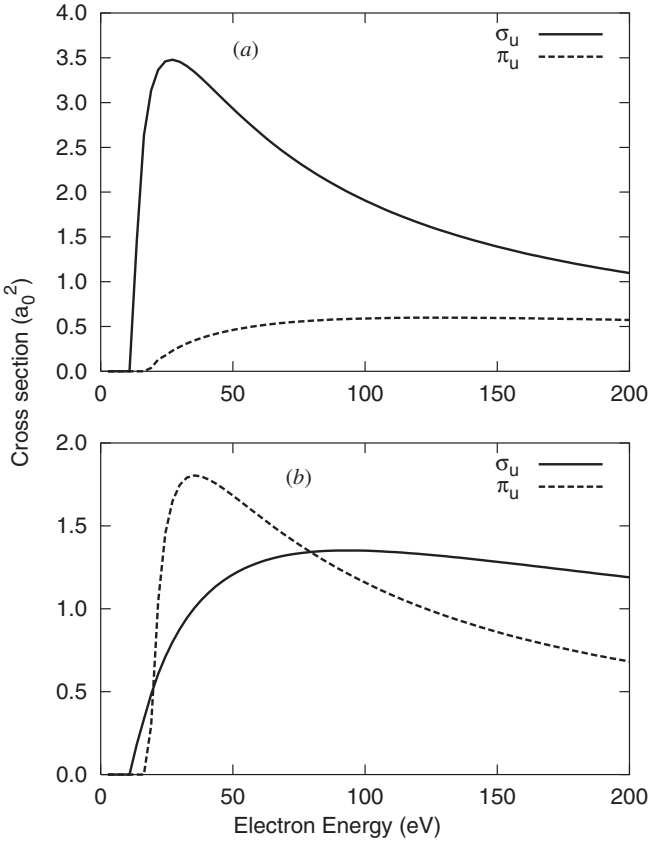

Figure 4. Electron impact excitation cross-sections to σ_u and π_u states of D_2^+ at the equilibrium distance. (*a*) The electron beam is parallel to the molecular axis; (*b*) the electron beam is perpendicular to the molecular axis.

the singlet cross-sections from the total cross-section following the empirical formula derived by Yudin and Ivanov [15] (their equations (8) and (9)).

These empirical formulae allow us to calculate electron impact excitation cross-sections from σ_g to σ_u and to π_u states at each internuclear separation and at each alignment angle of the D_2^+ ion. In figure 4 we compare the electron impact excitation cross-sections at the equilibrium distance to σ_u and π_u states, for D_2^+ ions lying parallel and perpendicular to the incident electron direction which is also the direction of the laser polarization, respectively. When D_2^+ is aligned parallel to the laser polarization, impact excitation to σ_u is the dominant channel. The π_u cross-sections are smaller due to two factors: (1) the π_u state has higher excitation energy; (2) the $2p_0$ state has larger cross-sections than $2p_1$ for the electron energies considered. The situation is different when the D_2^+ ion is aligned perpendicular to the laser polarization direction. Figure 4 (*b*) indicates that excitation to the π_u state is actually larger than that to the σ_u state, at least in the 20–80 eV energy region. Note that in the experiments of Niikura *et al*. [2, 3] the H_2^+ or D_2^+ were chosen to be perpendicular to the laser polarization direction. They assumed that electron impact excitation populates only the σ_u state, in disagreement with our analysis.

The semi-empirical formulae presented above allow us to calculate electron impact excitation cross-sections to σ_u and π_u states averaged over the initially randomly distributed D_2^+ ions. We obtained the ratio of the cross-section of σ_u with respect to π_u, and compared the result with the ratio obtained by Peek [19] where the impact excitation cross-sections for different internuclear separations were calculated using the Born approximation. The agreement is quite good, with the average cross-section for σ_u about a factor of two larger than for π_u. The absolute cross-sections from Peek are larger since the Born approximation was used.

We also consider the small contribution from excitation to the $2s\sigma_g$ electronic state of D_2^+. The empirical formula is chosen to be

$$\sigma_e(T, \Delta E) = \frac{1}{\Delta E^2} f(T/\Delta E), \tag{24}$$

$$f(x) = \frac{A}{1 + (B/x)} \frac{1}{x}, \tag{25}$$

where the parameters $A = 0.17$ and $B = 1.53$ are obtained by fitting the formula to the $1s \rightarrow 2s$ excitation cross-sections of H. This cross-section is assumed to be independent of the alignment of the molecular ion.

3. Results and discussion

As depicted in figure 1, we treat the first ionization by the MO-ADK model and the impact excitation and ionization by the rescattered electron is modelled using the semi-classical method introduced above. Once the other electron is in the exited states of D_2^+, it can be further ionized by the laser field, which can be treated by MO-ADK again, or it can dissociate directly into $D + D^+$, releasing kinetic energy for each atom or ion characteristic of the internuclear distance where the breakup is initiated.

The KER spectra of D^+ ions can be determined without any coincidence, as in the experiments of Niikura *et al*. [2, 3], or by detecting the two D^+ ions in

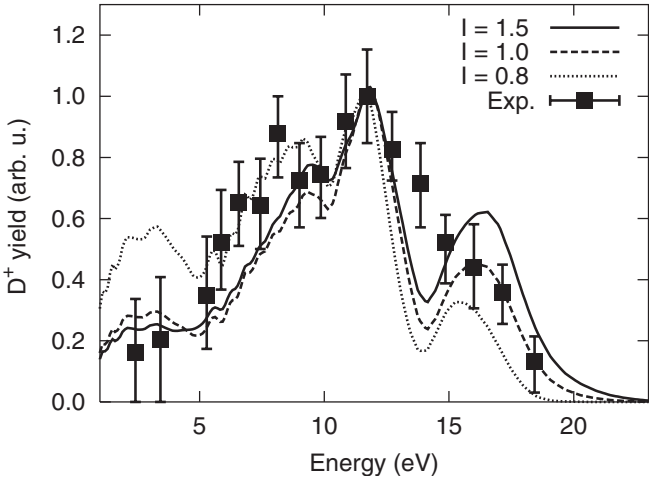

Figure 5. D^+ yield at several laser intensities for a 40 fs pulse length. The experimental data are from [3] for $1.5\,I_0$ where $I_0 = 10^{14}\,\mathrm{W\,cm^{-2}}$. The peak values from experiment and from theory for $1.5\,I_0$ are normalized to each other. For peak intensities of $1.0\,I_0$ and $0.8\,I_0$, the yields have been multiplied by 1.4 and 3.0, respectively, to have the same peak ion yield height.

coincidence, as in the experiments of Staudte *et al*. [1] or Alnaser *et al*. [4]. We will present our simulation results for both types of experiments.

3.1. *Non-coincidence D^+ KER spectra—dissociation or ionization?*

In the experiments of Niikura *et al*. [2, 3], the kinetic energy of D^+ ions was measured in the direction perpendicular to the direction of laser polarization. The measured non-coincidence D^+ signals come from ionization as well as from dissociation. Thus,

$$\text{Signal} \propto 2\frac{\mathrm{d}P_{\text{ion}}}{\mathrm{d}E} + \frac{\mathrm{d}P_{\text{dis}}}{\mathrm{d}E}. \tag{26}$$

In figure 5 the experimental D^+ kinetic energy spectra from Niikura *et al*. [3] are shown. The energy scale is the total breakup energy, or twice the energy of the D^+ ion. The experiment was performed for a pulse of 40 fs and peak intensity of $1.5\,I_0$. We have shown simulations with the same laser parameters but with three peak laser intensities, at 1.5, 1.0 and $0.8\,I_0$. First we normalize the peak height at 12 eV between theory and experimental data at $1.5\,I_0$. Since the peak positions do not vary with laser intensity, we can normalize the calculated spectra at the two other intensities as well, with a multiplicative factor of 1.4 and 3.0 for the 1.0 and $0.8\,I_0$, respectively. If one compares the experimental spectra with the theoretical ones calculated at the same $1.5\,I_0$, clearly the high energy peak near 16 eV from the theory is too high, while the theoretical spectra between 5 and 10 eV are somewhat too low. However it appears that the discrepancy can be reconciled if one takes into account the volume effect in that the experimental spectra have to be integrated over a volume where the intensities are less than the peak value. The energy resolution and the finite acceptance angles can all contribute to the smoother experimental spectra. One of course should also take this 'better agreement' with caution in view that the peak intensity of the laser is often not known precisely.

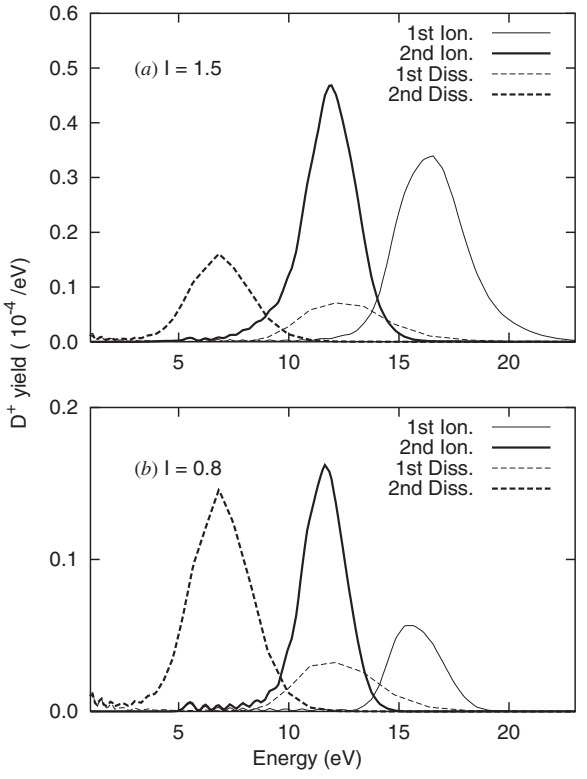

Figure 6. Decomposition of D^+ ion yields into contributions from dissociation and ionization, and for rescattering occurring within the first and the second optical cycle after the initial tunnelling ionization. The peak laser intensities are (*a*) $I = 1.5\,I_0$ and (*b*) $I = 0.8\,I_0$, where $I_0 = 10^{14}\,\mathrm{W\,cm^{-2}}$ and pulse length is 40 fs.

One of the major goals of the simulation is to unravel the origin of the structure in the kinetic energy spectra which in turn would provide insight into the working of the molecular clock. For this purpose, we show in figure 6 the calculated kinetic energy spectra, but separate the contributions from dissociation and ionization, and from rescattering occurring after one or two optical cycles, or equivalently, from the first (t_1) or the third returns (t_3), at two laser intensities, 1.5 and $0.8\,I_0$. At the higher intensity, in this figure we notice: (1) ionization is much stronger than dissociation; (2) the peak from the third return (2nd cycle) is higher than from the first return; (3) the width of the peak from the first return is broader than the peak from the third return. Another interesting observation is that the peak position of the dissociation spectra from the first return almost coincides with the peak position in the ionization spectra from the third return. This shift is due to the binding energy of the excited electronic states.

In the experiment of Niikura *et al.* [3] the peak at 12 eV was attributed to originate from the dissociation of D_2^+ via the σ_u curve at the first return. In other words, this peak reads the clock at t_1. According to our simulation, the peak comes from ionization following rescattering at the third return, and this peak should read the clock at t_3.

Contributions to the D^+ signal from dissociation do become more important at lower laser intensity, as shown in figure 6 (*b*). Even at this intensity, the peak at

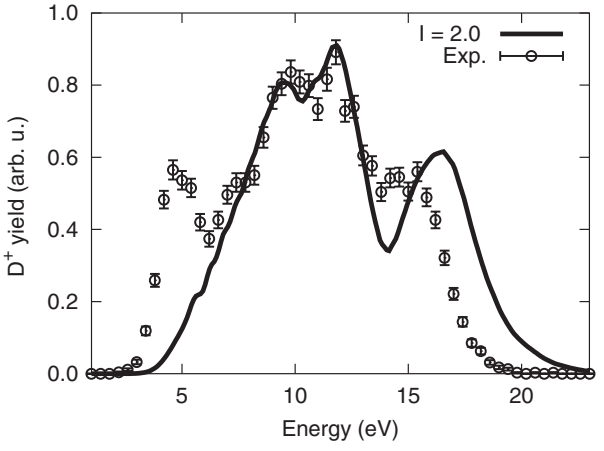

Figure 7. Comparison of D^+ ion spectra resulting from the double ionization of D_2 molecules in a laser field. The experiment data are from [4] for peak laser intensity of $2.8\,I_0$ and the theoretical simulation is for laser peak intensity of $2.0\,I_0$, where $I_0 = 10^{14}\,\mathrm{W\,cm^{-2}}$ and the pulse length is 35 fs.

12 eV still comes mostly from the ionization following rescattering at t_3 instead of dissociation following rescattering at t_1. Furthermore the third return peak is higher than the first return peak for either dissociation or ionization. We remark that the spectra in figure 5 were calculated including contributions up to four or five optical cycles after the initial tunnelling ionization and convergence of the calculation had been checked.

3.2. *Coincidence KER spectra*

The D^+ ion kinetic energy distributions in laser–D_2 interactions have been determined in coincidence measurements where the two D^+ ions were detected simultaneously by Staudte *et al.* [1] and more recently by Alnaser *et al.* [4]. In the latter experiment, the branching ratios of ionization with respect to dissociation had been measured as well, for peak laser intensities of $1–5\,I_0$. Their data for peak intensity of $2.8\,I_0$ are shown in figure 7. The experiment used a 35 fs pulse with mean wavelength of 800 nm. The D^+ spectra are from Coulomb explosion of ions at 60°–80° with respect to the direction of the linear polarization of the laser field. In the figure we show the result of our theoretical simulation for laser intensity of $2.0\,I_0$. We found best overall agreement with the experimental data at this intensity without considering the volume effect and the fact that the theoretical calculation was carried out for molecules aligned perpendicular to the laser polarization while the experiments measured ions coming out of 60°–80° with respect to the laser polarization. The simulated spectra near the kinetic energy peak region of 7–12 eV agree quite well with the data, but the peak near 17 eV is more pronounced in the simulation. We attribute the discrepancy to the volume effect as in the non-coincidence experiments.

4. Summary and conclusion

In this paper we have provided a comprehensive study of the elementary processes of the rescattering mechanism leading to the fragmentation of D_2^+

following the initial tunnelling ionization of a D_2 molecule in a short intense laser pulse. Ionization rates of D_2^+ from the excited electronic states and impact excitation and ionization cross-sections by the returning electron have been obtained based on the MO-ADK theory and from semi-empirical formulae, respectively. Following the initial idea of Corkum and co-workers, we showed that the kinetic energy spectra of D^+ in the higher energy region (5 to 10 eV per D^+ ion) can be used as a molecular clock which can be read with sub-femtosecond accuracy. Through our detailed simulation, we concluded that the dominant peak in the D^+ kinetic energy spectrum is due to the further ionization of the excited D_2^+ following impact excitation by the returning electron, and this excitation occurs not at the first return but mostly at the third return. We have compared our simulation results with the recent experiments of Niikura *et al*. and of Alnaser *et al*. with general good agreement. Further experimental studies in terms of dependence on laser wavelength, pulse duration and alignment angles may provide a more critical test of the present theoretical model. From the theoretical viewpoint, despite of the semi-empirical nature of the present modelling, we do not expect any meaningful pure *ab initio* quantum calculations to be viable in the foreseeable future. The present model has the further advantage that the mechanism for producing individual peaks in the kinetic energy spectra can be identified and the effect of laser parameters can be readily tested. On the other hand, the semi-empirical nature of the modelling can claim its reliability only after it has been exposed to more stringent tests from experiment.

Acknowledgments

This work is in part supported by Chemical Sciences, Geosciences and Biosciences Division, Office of Basic Energy Sciences, Office of Science, US Department of Energy. CDL also wishes to thank Igor Bray for communicating to him the partial $1s \rightarrow 2p_m$ ($m = 0, 1$) cross-sections.

References

[1] Staudte, A., Cocke, C. L., Prior, M. H., Belkacem, A., Ray, C., Chong, H. W., Glover, T. E., Schoenlein, R. W., and Saalmann, U., 2002, *Phys. Rev.* A, **65,** 020703(R).
[2] Niikura, H., Legare, F., Hasbani, R., Bandrauk, A. D., Ivanov, M. Y., Villeneuve, D. M., and Corkum, P. B., 2002, *Nature*, **417,** 917.
[3] Niikura, H., Legare, F., Hasbani, R., Ivanov, M. Y., Villeneuve, D. M., and Corkum, P. B., 2003, *Nature*, **421,** 826.
[4] Alnaser, A. S., Osipov, T., Benis, E. P., Wech, A., Cocke, C. L., Tong, X. M., and Lin, C. D., 2003, *Phys. Rev. Lett*., **91,** 163002.
[5] Smirnov, B. M., and Chibisov, M. I., 1966, *Zh. Eksp. Teor. Fiz*., **49,** 841.
[6] Perelomov, A. M., Popov, V. S., and Terentev, M. V., 1966, *Zh. Eksp. Teor. Fiz*., **50,** 1393.
[7] Ammosov, M. V., Delone, N. B., and Krainov, V. P., 1986, *Zh. Eksp. Teor. Fiz*., **91,** 2008.
[8] Dill, D., and Dehmer, J. L., 1974, *J. chem. Phys*., **61,** 692.
[9] Liang, X. L., Pan, X. C., and Li, J. M., 1985, *Chin. Phys. Lett*., **2,** 545.
[10] Tong, X. M., Zhao, Z. X., and Lin, C. D., 2002, *Phys. Rev.* A, **66,** 033402.
[11] Zhao, Z. X., Tong, X. M., and Lin, C. D., 2003, *Phys. Rev.* A, **67,** 043404.
[12] Litvinyuk, I. V., Lee, K. F., Dooley, P. W., Rayner, D. M., Villeneuve, D. M., and Corkum, P. B., 2003, *Phys. Rev. Lett*., **90,** 233003.
[13] Chu, X., and Chu, S. I., 2001. *Phys. Rev.* A, **63,** 013414.

[14] YUDIN, G. L., and IVANOV, M. Y., 2001, *Phys. Rev.* A, **63,** 033404.
[15] YUDIN, G. L., and IVANOV, M. Y., 2001, *Phys. Rev.* A, **64,** 035401.
[16] FU, L. B., LIU, J., CHEN, J., and CHEN, S. G., 2001, *Phys. Rev.* A, **63,** 043416.
[17] BRAY, I., CCC-database, http://atom.murdoch.edu.au/CCC-WWW/index.html.
[18] KIM, Y. K., IRIKURA, K. K., and ALI, M. A., 2000, *J. Res. NIST*, **105,** 285.
[19] PEEK, J. M., 1964, *Phys. Rev.*, **134,** A877.